

An indirect measurement of gas evolution in galaxies at $0.5 \leq z \leq 2.0$

G. Popping^{1*}, K.I. Caputi^{2,1}, R.S. Somerville³, and S.C. Trager¹

¹*Kapteyn Astronomical Institute, University of Groningen, Postbus 800, NL-9700 AV Groningen, the Netherlands*

²*Scottish Universities Physics Alliance (SUPA), Institute for Astronomy, The University of Edinburgh, Royal Observatory, Edinburgh EH9 3HJ*

³*Department of Physics and Astronomy, Rutgers University, 136 Frelinghuysen Road, Piscataway, NJ 08854, USA*

January 19, 2012

ABSTRACT

One key piece of information missing from high redshift galaxy surveys is the galaxies' cold gas contents. We present a new method to indirectly determine cold gas surface densities and integrated gas masses from galaxy star formation rates and to separate the atomic and molecular gas components. Our predicted molecular and total gas surface densities and integrated masses are in very good agreement with direct measurements quoted in the literature for low and high- z galaxies. We apply this method to predict the gas content for a sample of ~ 57000 galaxies in the *COSMOS* field at $0.5 < z < 2.0$, selected to have $I_{AB} < 24$ mag. This approach allows us to investigate in detail the redshift evolution of galaxy cold and molecular gas content versus stellar mass and to provide fitting formulae for galaxy gas fractions. We find a clear trend between galaxy gas fraction, molecular gas fraction and stellar mass with redshift, suggesting that massive galaxies consume and/or expel their gas at higher redshift than less massive objects and have lower fractions of their gas in molecular form. The characteristic stellar mass separating gas- from stellar-dominated galaxies decreases with time. This indicates that massive galaxies reach a gas-poor state earlier than less massive objects. These trends can be considered to be another manifestation of downsizing in star formation activity.

Key words: galaxies: evolution - galaxies: formation - galaxies: ISM - ISM: molecules

1 INTRODUCTION

In a pioneering work, Madau et al. (1996) demonstrated that the star formation (SF) activity of the Universe peaks at a redshift $z \sim 1 - 3$ and decreases at lower redshifts to its present day value. In the following years, many studies confirmed the existence of a peak in the star formation rate (SFR) density around these redshifts, and a clear decline at $z < 1$ (e.g., Hopkins 2004; Hopkins & Beacom 2006). This makes the epoch between $z \sim 2$ and $z \sim 0.5$, in which massive galaxies stop forming the bulk of their stars and become passive, a crucial period for galaxy evolution.

One of the features which has become clear in this period of galaxy evolution is that the most massive objects (giant elliptical galaxies hosted in galaxy groups and clusters) formed their stars early, while less massive objects continued to form stars until the present (this trend is commonly called ‘galaxy downsizing’). This behavior has many different observa-

tional manifestations (e.g., Faber, Worthey & Gonzales 1992; Worthey, Faber & Gonzalez 1992; Cowie et al. 1996; Trager et al. 2000; Drory et al. 2004, 2005; Cimatti, Daddi & Renzini 2006; Trager, Faber & Dressler 2008), but its physical origin remains unclear (Fontanot et al. 2009).

The star formation rate in galaxies is closely linked to the galaxy gas content. Observations have shown that SF in the Milky Way takes place in dense, massive and cold giant molecular clouds (GMC; Solomon et al. 1987; Bolatto et al. 2008; McKee & Ostriker 2007). This makes the SF tightly connected to the molecular and atomic gas available. Schmidt (1959) found a power-law relation between the surface density of SFR and gas surface density. This work has become the cornerstone of a wealth of studies relating SFR surface densities and cold gas and molecular hydrogen surface densities (e.g., Kennicutt 1998b; Bigiel et al. 2008; Schruba et al. 2011). Both the observations of GMCs, and the power-law relations between SFR and gas densities demonstrate that information about the gas and its partition into atomic and molecular hydrogen is

* E-mail: G.Popping@astro.rug.nl

essential for a proper understanding of galaxy evolution and the build up of stellar mass.

An essential landmark and significant step forward in the study of galaxy evolution at higher redshifts has been the development of large samples of distant galaxies with extensive multi-wavelength information (e.g., *GOODS* and *COSMOS*). These samples comprise imaging data from X-rays to the infrared, which allow us to derive numerous physical properties of galaxies, such as stellar masses and star formation rates. However, one of the key pieces of information missing in these studies is the cold gas content. Deriving the amount of cold gas present as a function of stellar mass for large representative samples would allow us to better understand the history of gas consumption and the overall phenomenon of galaxy downsizing.

Information about the gas content of galaxies also provides important constraints on theoretical models of galaxy formation. Gas fractions help to break the degeneracies in different physical mechanisms that are included in these models, namely star formation and stellar feedback (Caviglia & Somerville, in prep). Moreover, cosmological galaxy formation models have begun to include recipes that allow a detailed tracking of atomic and molecular gas with redshift in the context of general galaxy properties (e.g., gas mass functions, gas properties as a function of stellar mass; Obreschkow & Rawlings 2009; Fu et al. 2010; Gnedin & Kravtsov 2011; Krumholz & Dekel 2011; Kuhlen et al. 2011; Lagos et al. 2011b,a, Popping et al., in prep). Observational constraints on atomic and molecular gas content as a function of galaxy properties and cosmic time are crucial for developing and calibrating these new models.

Direct observational measurements of the gas content in distant galaxies are currently available for only a very limited number of galaxies, and are likely biased towards the most gas-rich objects. Gas is usually detected using CO molecules as a tracer, so no direct information about the atomic gas content of high redshift galaxies is currently available. In addition, the conversion from CO to molecular hydrogen mass is notoriously uncertain and may depend on galaxy properties (Genzel et al. 2010, and references therein). In the coming decade, it is hoped that new facilities like ALMA (Atacama Large Millimeter array) and the SKA (Square Kilometer Array) will reveal the gas content in representative samples of high-redshift galaxies.

In the meantime, we can obtain *indirect* constraints on gas content by using the observational estimates of galaxy size and SFR and empirical correlations between SFR density and gas density. This approach has been used by Erb et al. (2006) and Mannucci et al. (2009), who obtained estimates of gas masses for high redshift galaxies by inverting the Schmidt-Kennicutt relation (KS law) described in Kennicutt (1998b), which relates SFR surface density to the combined atomic and molecular hydrogen surface density. However, the indirect estimates of gas fraction that they obtain do not agree well with the direct measurements, as we later show. This could be because the direct estimates are biased high, or it could be that the “total gas” form of the KS law does not apply. It has been shown that the KS law breaks down at the lowest gas surface densities (Bigiel et al. 2008). This breakdown is ascribed to the inability of the cold gas at low surface densities to collapse

gravitationally and form molecular clouds from which stars may originate. SFR surface density correlates in an almost linear fashion with the molecular gas surface density without breaking down at lower surface densities (Bigiel et al. 2008, 2011; Schruha et al. 2011). Using an inverted *molecular-gas-based SF law* therefore seems more appropriate to probe the cold gas content of high-redshift galaxies. Furthermore, inverting a molecular-gas-based SF law allows for comparison between directly and indirectly measured molecular gas masses of high-redshift galaxies.

In this paper we present an improved method to derive the gas properties of distant galaxies from their star formation rate densities. An integral part of our new method is a prescription to calculate the molecular fraction of cold gas based on the results by Blitz & Rosolowsky (2006). These authors found that the ratio between the molecular and atomic hydrogen surface density ($R_{H_2} = \Sigma_{H_2}/\Sigma_{HI}$) in discs can be described empirically as a function of the hydrostatic mid-plane pressure P_m , driven by the stellar and gas density (see also Wong & Blitz 2002; Blitz & Rosolowsky 2004). This allows us to invert the much tighter and more physical molecular gas based star formation relation derived for nearby galaxies by Bigiel et al. (2008), instead of the traditional KS relation.

We apply our method to ~ 57000 galaxies from the *COSMOS* survey in the redshift range of $0.5 \leq z \leq 2.0$ to study the structure and properties of gas and the galaxy evolution over this important cosmic epoch. *COSMOS* was chosen for our study because it has well established disc sizes based on high resolution (Hubble Space Telescope) imaging, crucial for our method, imaging running from the X-ray to radio wavelengths to derive stellar masses and SFR, and spans a wide range of redshift.

The outline of this paper is as follows. In Section 2, we present our method to indirectly measure the molecular and the total cold gas content in galaxies. In Section 3, we apply this method to both low- and high-redshift data with known gas properties and calibrate our results against direct measures of cold and molecular gas. In Section 4, we describe the application of the developed method to $\sim 57,000$ galaxies from the *COSMOS* survey in the redshift range of $0.5 \leq z \leq 2.0$, and the resulting gas properties with respect to other galaxy parameters. We discuss our findings in Section 5 and summarize our results in Section 6. Throughout the paper we apply a Λ CDM cosmology with $H_0 = 70 \text{ km s}^{-1}$, $\Omega_{\text{matter}} = 0.28$, and $\Omega_{\Lambda} = 0.72$. We assume a universal Chabrier stellar initial mass function (IMF: Chabrier 2003) and where necessary convert all observations used to a Chabrier IMF. All presented cold and molecular gas surface densities and integrated masses include a correction of 1.36 to account for Helium.

2 METHOD

2.1 Calculating gas surface densities

We infer gas surface densities using a combination of an empirical molecular star formation law (based on Bigiel et al. 2008) and a prescription to calculate the fraction of molecular hydrogen in cold gas (based on Blitz & Rosolowsky 2006).

Table 1. Summary of the parameters used in our indirect gas measure method. These parameters lead to the overall best fit results for integrated masses in Section 3

Parameter	Description	Value	Reference
A_{SF}	Normalization of the star formation law ($M_{\odot} \text{ yr}^{-1} \text{ kpc}^{-2}$)	1.09×10^{-2}	Sec. 3.3
N_{SF}	Index which sets star formation efficiency	0.5	Sec. 3.3
Σ_{crit}	Critical surface density which sets star formation efficiency ($M_{\odot} \text{ pc}^{-2}$)	100	Sec. 3.3
P_0	Normalization of the Blitz & Rosolowsky (2006) power-law	2.35×10^{-13}	Leroy et al. (2008)
α	Index of the Blitz & Rosolowsky (2006) power-law	0.8	Leroy et al. (2008)
\bar{f}_{σ}	Mean ratio between gas and stellar vertical velocity dispersion in the stellar disc	0.4	Elmegreen (1993)
χ_{gas}	Scale radius of the gas disc, relative to the stellar disc	1.5	Sec. 3.3

We have slightly adapted the star formation law deduced by Bigiel et al. (2008) to allow for higher star formation efficiencies in high gas surface density regions. This is based on the results of Daddi et al. (2010) and Genzel et al. (2010), who found the star-formation at high surface densities to follow the KS - law (power-law slope of 1.4 versus 1.0 for Bigiel et al. (2008)). The resulting equation is given by

$$\Sigma_{\text{SFR}} = \frac{A_{\text{SF}}}{10 M_{\odot} \text{ pc}^{-2}} \left(1 + \frac{\Sigma_{\text{gas}}}{\Sigma_{\text{crit}}} \right)^{N_{\text{SF}}} f_{\text{H}_2} \Sigma_{\text{gas}} \quad (1)$$

where Σ_{SFR} and Σ_{gas} are the star formation and cold gas surface densities in $M_{\odot} \text{ yr}^{-1} \text{ kpc}^{-2}$ and $M_{\odot} \text{ pc}^{-2}$, respectively, A_{SF} is the normalization of the power law in $M_{\odot} \text{ yr}^{-1} \text{ kpc}^{-2}$, Σ_{crit} a critical surface density above which the star formation follows Kennicutt (1998b), N_{SF} is an index which sets the efficiency, and $f_{\text{H}_2} = \Sigma_{\text{H}_2} / (\Sigma_{\text{HI}} + \Sigma_{\text{H}_2})$ is the molecular gas fraction. Table 1 gives a summary of the parameter values and their origin.

Given a star-formation surface density, this equation can be solved for the cold gas surface density when one knows the molecular fraction of the cold gas. We use a pressure-regulated recipe to determine the molecular fraction of the cold gas, based on the work by Blitz & Rosolowsky (2006). They found a power-law relation between the mid-plane pressure acting on a galaxy disc and the ratio between molecular and atomic hydrogen, i.e.,

$$R_{\text{H}_2} = \left(\frac{\Sigma_{\text{H}_2}}{\Sigma_{\text{HI}}} \right) = \left(\frac{P_m}{k_B P_0} \right)^{\alpha} \quad (2)$$

with P_0 the external pressure in the interstellar medium where the molecular fraction is unity. α and k_B are the power-law index and the Boltzmann constant, respectively (see Table 1). P_m is the mid-plane pressure acting on the galaxy disc, and is given by (Elmegreen 1989)

$$P_m(r) = \frac{\pi}{2} G \Sigma_{\text{gas}}(r) (\Sigma_{\text{gas}}(r) + f_{\sigma}(r) \Sigma_{*}(r)) \quad (3)$$

where G is the gravitational constant, r is the radius from the galaxy centre, and $f_{\sigma}(r)$ is the ratio between $\sigma_{\text{gas}}(r)$ and $\sigma_{*}(r)$, the gas and stellar vertical velocity dispersion, respectively. We followed the method presented in Fu et al. (2010) to determine f_{σ} as a function of radius r . Observations have shown that σ_{gas} remains constant over the disc (e.g. Shostak & van der Kruit 1984; Leroy et al. 2008). The stellar vertical velocity dispersion σ_{*} decreases exponentially and has a scale length twice the stellar disc scale length r_{*} (e.g. Bottema 1993), i.e.

$$\sigma_{*}(r) = \sigma_{*}^0 \exp(-r/2r_{*}) \quad (4)$$

where the stellar velocity dispersion in the center of the disc

is noted as σ_{*}^0 . The stellar mass surface density of an exponential disc is given by $\Sigma_{*} = \Sigma_{*}^0 \exp(-r/r_{*})$, which we can combine with the previous equation to find

$$f_{\sigma}(r) = \frac{\sigma_{\text{gas}}}{\sigma_{*}^0} \sqrt{\frac{\Sigma_{*}^0}{\Sigma_{*}(r)}} \equiv \bar{f}_{\sigma} \sqrt{\frac{\Sigma_{*}^0}{\Sigma_{*}(r)}} \quad (5)$$

where \bar{f}_{σ} is the ratio between the gas and stellar vertical velocity dispersion at the centre of the disc and Σ_{*}^0 is the stellar mass surface density in the centre of the disc. We can express \bar{f}_{σ} in terms of the mean value of $f_{\sigma}(r)$ in the disc by

$$\bar{f}_{\sigma} = \frac{\int 2\pi r \Sigma_{*}(r) f_{\sigma}(r) dr}{\int 2\pi r \Sigma_{*}(r) dr} \quad (6)$$

Substituting for $f_{\sigma}(r)$ and afterwards integrating we find

$$\bar{f}_{\sigma} = 4\bar{f}_{\sigma}^0. \quad (7)$$

By combining Equation (3) and Equation (5) we find

$$P_m(r) = \frac{\pi}{2} G \Sigma_{\text{gas}}(r) \left(\Sigma_{\text{gas}}(r) + \frac{\bar{f}_{\sigma}}{4} \sqrt{\Sigma_{*}(r) \Sigma_{*}^0} \right) \quad (8)$$

We now have all the necessary ingredients to calculate R_{H_2} and subsequently the cold gas molecular fraction [$f_{\text{H}_2} = R_{\text{H}_2} / (1 + R_{\text{H}_2})$].

Putting this together, we have an expression for the star formation law depending on the cold gas surface density, stellar mass surface density and stellar mass and scale length of the disc. Given a star formation surface density and stellar surface-density, we can now indirectly determine the cold gas surface density through iteration. The molecular gas fraction, and subsequently the molecular gas surface density, can then easily be calculated from Equation (2), using the stellar mass surface density and previously determined gas surface density as input.

Intrinsically hidden in this method is the CO-to- H_2 conversion factor (X_{CO}). This conversion factor was used to determine 1) the normalization constant A_{SF} for the empirical star formation law based on H_2 (Bigiel et al. 2008) and 2) the ratio between molecular and atomic hydrogen R_{H_2} which was used to determine the normalization and power-law index for the pressure-based H_2 fraction recipe (Leroy et al. 2008). However, Blitz & Rosolowsky (2006) proposed that changes in the CO-to- H_2 conversion factor are unlikely to substantially alter results for the latter point. Unless stated differently, we adopted a value of $X_{\text{CO}} = 2.0 \times 10^{20} \text{ cm}^{-2} (\text{K km s}^{-1})^{-1}$.

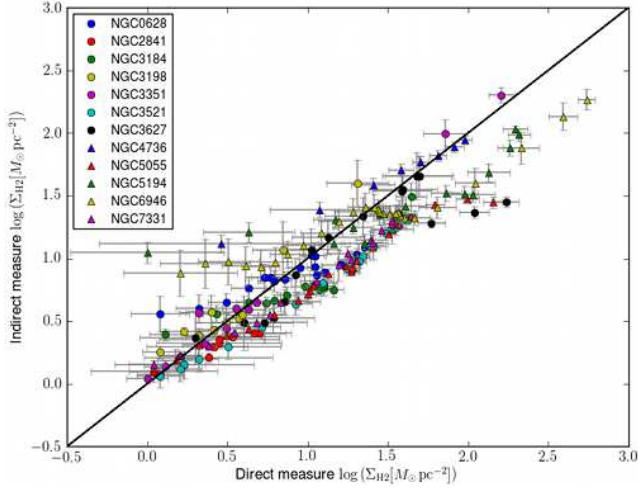


Figure 1. Comparison between indirect and direct measures of molecular gas surface densities, taken from the radial profiles of the THINGS galaxies (Leroy et al. 2008) using our method. All datapoints are coded by galaxy and represent surface densities sampled along their host galaxy radius.

2.2 Constructing a galaxy

The method described in the previous subsection allows one to calculate the gas surface density, given a measured stellar-mass surface density and SFR surface density. However, for many high-redshift objects only global parameters are available, combined with some morphological information (e.g., stellar scale length r_* , half light radius $r_{0.5}$).

In order to calculate the cold and molecular gas content of these galaxies, we distribute the stellar mass into an exponential disc following $\Sigma_*(r) = \Sigma_*^0 \exp(-r/r_*)$ where r_* is the scale length of the stellar disc and Σ_*^0 is the stellar mass surface density in the centre of the disc (defined as $\Sigma_*^0 = M_*/(2\pi r_*^2)$ where M_* is the galaxy stellar mass). The star formation in the galaxy is distributed similarly, with a disc scale length

$$r_{\text{gas}} = \chi_{\text{gas}} r_*, \quad (9)$$

where χ_{gas} is a scale radius of the gas disc relative to the stellar disc (see Table 1). The use of χ_{gas} is motivated by the radial extent of H I gas in spiral galaxies (Broeils & Rhee 1997). A galaxy’s total cold gas budget can be found by integrating over the inferred gas surface densities. We find the best fit results for integrated masses (see Section 3.2) when distributing the stellar mass and star formation over an exponential disc out to five times the stellar disc scale length.

3 CALIBRATION OF THE METHOD

In this section we compare indirect measures of gas surface densities and integrated masses obtained using the method presented in the previous section to direct measures from the literature. Results were obtained using the parameter values as summarized in Table 1. Note that the purpose of this method was to measure the global cold gas and molecular content of galaxies, rather than local surface densities. Parameters were chosen to best achieve this purpose. We

discuss the effects of changing the parameters in Section 3.3.

3.1 Local galaxy surface densities

Figures 1 and 2 show total cold gas and molecular gas surface densities obtained using our method. The indirect measures were computed from the radial profiles of the star-formation surface densities and stellar mass surface densities, in combination with the host galaxy total mass and stellar scale length all obtained from Leroy et al. (2008). These predictions are plotted against literature values for total cold gas and molecular gas surface densities taken from Leroy et al. (2008)

We find good general agreement between results obtained using our method and literature values at molecular surface densities ranging from $\Sigma_{\text{H}_2} \sim 1$ to $\Sigma_{\text{H}_2} \sim 300 M_\odot \text{pc}^{-2}$ (Figure 1). There is a scatter around the one-to-one line of 0.1 to 0.3 dex at the lowest and more intermediate surface densities, respectively. We overestimate the lowest molecular surface densities for NGC 6946 and NGC 5194, whereas we under-predict at high surface densities for these galaxies (also see NGC 3627). The star-formation efficiency (SFE, the ratio of SFR over molecular gas) of these galaxies decreases significantly towards smaller radii (at the highest surface densities) compared to the predicted SFE from the mid-plane pressure on the disc (see Appendix F of Leroy et al. 2008). The low SFE of these galaxies with respect to theoretical values will result in the observed surplus of molecular gas as predicted by our method. Opposite behavior is observed for these galaxies towards larger radii, where the molecular surface density is much lower. In this case, deviations between observed and theoretical SFE result in a deficit of molecular hydrogen as computed by our method.

We also find very good agreement between the total gas surface densities computed using our method and surface densities obtained from the literature (left-hand panel of Figure 2), with smaller scatter especially at the lower gas surface densities. We predict a deficit of total cold gas compared to literature values at the highest surface densities. Similar to the molecular gas surface densities, we ascribe this deficit to differences between theoretically predicted and observed SFE. Overall we find a mean ratio of $\Sigma_{\text{gas indirect}}/\Sigma_{\text{gas observed}} = 0.94$ with a standard deviation of 0.021 for our method.

We plot indirect total cold gas surface densities obtained with the KS law as a function of the literature values in the right-hand panel of Figure 2 for comparison. Although the scatter around the one-to-one line of the two methods is similar, there is a clear offset from this line when using the KS law, resulting in a general deficit of gas over the entire range of total gas surface densities. We find a mean ratio $\Sigma_{\text{gas indirect}}/\Sigma_{\text{gas observed}} = 0.79$ with a standard deviation of 0.019 when using the KS law for the indirect gas measure. This was expected for the lowest surface densities where the KS law breaks down (Bigiel et al. 2008), which also appears in Figure 2. However, the offset is surprising at the higher gas surface densities at which the KS law is defined to relate SFR surface densities with the total gas surface density. Putting the observed gas surface densities in $\Sigma_{\text{SFR}} - \Sigma_{\text{gas}}$ space and comparing with the KS law shows that the data lie

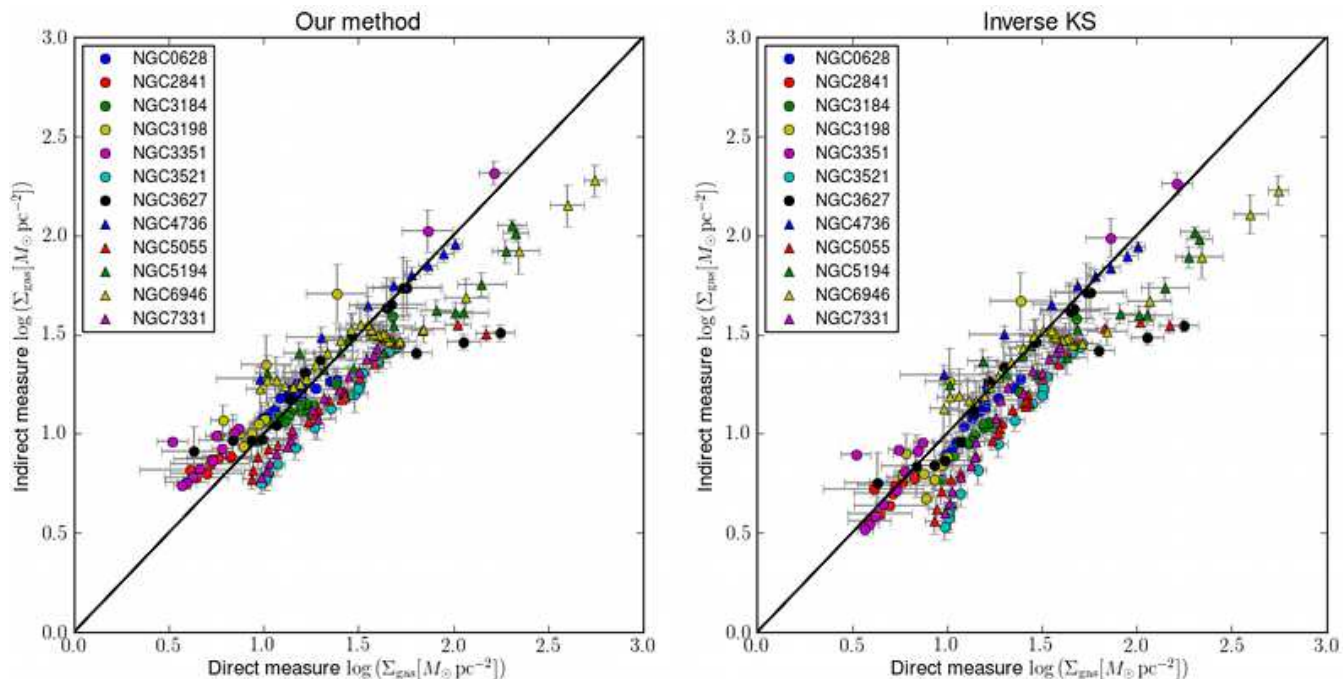


Figure 2. Indirect versus direct measures of total cold gas surface densities, taken from the radial profiles of the THINGS galaxies (Leroy et al. 2008). Left and right panel using our and the KS indirect gas measure method, respectively. We find better agreement with literature values than the indirect KS method, especially at low surface densities.

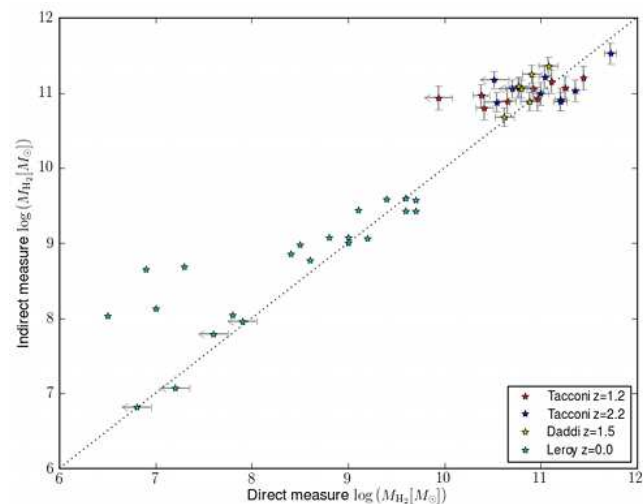


Figure 3. Indirect vs. direct measures of galaxy molecular gas masses using our indirect gas method. Both low- (Leroy et al. 2008) and high- (Tacconi et al. 2010; Daddi et al. 2010) redshift galaxies are displayed. Apart from four local dwarf galaxies (see Sec. 3.2), we find good agreement between literature values and our method at all redshifts and molecular gas masses.

slightly below the KS law. Nevertheless, this can not account for the breakdown at low gas surface densities. We therefore find that our method yields the biggest improvements at the lowest gas surface densities (i.e., the outer parts of galaxy discs).

3.2 Galaxy integrated gas masses

We present galaxy integrated H_2 and total cold gas masses obtained with our method versus literature values in Figures 3 and 4, respectively. We applied our method to a small sample of both low and high-redshift galaxies, compiled from Leroy et al. (2008, $z = 0$), Daddi et al. (2010, $z \sim 1.5$), and Tacconi et al. (2010, $z \sim 1.2$ and $z \sim 2.2$). We applied the X_{CO} factors as determined by the latter two authors for their galaxy samples [$X_{CO} \sim 2.5 \times 10^{20}$ and $X_{CO} = 2.0 \times 10^{20} \text{ cm}^{-2} (\text{K km s}^{-1})^{-1}$, respectively].

We find good agreement between our results and observations over the entire range of H_2 masses and redshifts. There is a slight excess of H_2 computed with our method as compared to the direct measurements (~ 0.2 dex; Figure 3). We find a spread of ~ 0.25 dex around the mean trend in computed versus literature H_2 masses. We neglect the four local galaxies with a surplus of integrated H_2 masses of 1–1.5 dex. All four are classified as dwarf galaxies and have anomalously high SFE in their central parts (Leroy et al. 2008). These authors argue for an unaccounted-for reservoir of H_2 in these galaxies, possibly due to variations in the X_{CO} factor for dwarfs with respect to bigger spiral galaxies (see also Spaans & Norman 1997). We find one clear outlier at higher redshift, with an upper limit on its observed H_2 mass. It is most likely that this galaxy also has a high SFE we cannot account for.

Current instruments do not allow for atomic hydrogen observations at high redshifts. We are therefore restricted to local galaxies when comparing literature values to total integrated galaxy gas masses computed with the method presented in this study. We find good agreement between our results and the observational data, although with a slight mean deficit (left-hand panel of Figure 4). We found a max-

imum deviation in literature values and our results of ~ 0.5 dex. Predicted cold gas masses for most galaxies are within ~ 0.3 dex of their literature values. It is worth noting that the four dwarfs for which we over-predict integrated H_2 masses are also included in this figure and have predicted total gas masses in good agreement with the observations. Although this seems promising, it means that not only do we find a surplus of H_2 compared to current literature studies, we also find a deficit of atomic hydrogen.

In the right hand panel of Figure 4 we present indirect total cold gas measures for local galaxies obtained by applying the KS law. Similar to the surface density profiles, the KS law predicts a deficit of total integrated gas mass. The outer parts of the galaxies (where the gas surface densities are lowest, the KS law breaks down and more gas is necessary to sustain SF) drive this deficit. Here we clearly see the strength of our method over previous indirect gas methods.

These results demonstrate out that our method can be used as a useful tool to predict the cold and molecular gas surface densities, as well as integrated gas masses for low- and high-redshift galaxies.

3.3 Changing parameters

The method presented in this paper has several free parameters, which all individually affect the outcome of indirect gas measures. In this subsection we explore the spread in results due to variations in free parameters.

We find that our method is robust against changes in the mean ratio between gas and stellar vertical velocity dispersion \bar{f}_σ . We explore values ranging from 0.1 to 2.0 and find differences in total cold gas surface density measures up to ~ 0.1 dex with respect to results obtained using the quoted value for \bar{f}_σ in Table (1). Differences are most prominent at the lowest gas surface densities ($\Sigma_{\text{gas}} \leq 10 M_\odot \text{pc}^{-2}$). The spread in integrated total cold gas masses due to changes in \bar{f}_σ also reaches only ~ 0.1 dex over the entire mass range probed by our control sample of galaxies. Changing \bar{f}_σ does not significantly affect molecular gas surface densities and integrated masses.

Blitz & Rosolowsky (2006) derived a power-law index α and a normalization constant P_0 slightly different than those we use ($\alpha = 0.8$ versus 0.92 and $P_0 = 5.93 \times 10^{-13}$ versus 2.35×10^{-13} , respectively). Applying their values to our method results in small changes of only ~ 0.1 dex at lower gas surface densities with respect to indirect gas measures obtained using the parameters as summarized in Table 1. Integrated gas masses differ within ~ 0.15 dex over the entire mass range probed.

The most significant changes in inferred indirect gas measures are due to variations in the normalization of the star formation law A_{SF} . In recent works Bigiel et al. (2008) and Bigiel et al. (2011) found values for the star formation normalization of $A_{\text{SF}} = 8.42 \times 10^{-3} M_\odot \text{yr}^{-1} \text{kpc}^{-2}$ and $A_{\text{SF}} = 4.6 \times 10^{-3} M_\odot \text{yr}^{-1} \text{kpc}^{-2}$, respectively (after conversion to a Chabrier IMF). We explored a range of parameters around these values and applied a χ^2 test on the derived integrated molecular and atomic gas masses (excluding dwarf galaxies). This resulted in a best fit value of $A_{\text{SF}} = 8.4 \times 10^{-3} M_\odot \text{yr}^{-1} \text{kpc}^{-2}$ for the integrated total cold gas masses, and $A_{\text{SF}} = 13.5 \times 10^{-3} M_\odot \text{yr}^{-1} \text{kpc}^{-2}$ for the integrated molecular gas masses. We found that

$A_{\text{SF}} = 10.9 \times 10^{-3} M_\odot \text{yr}^{-1} \text{kpc}^{-2}$ leads to best overall agreement between direct and indirect measures for both the total cold and molecular gas integrated masses (see Table 1).

Adopting other values (running from $A_{\text{SF}} = 1.0 \times 10^{-3}$ to $A_{\text{SF}} = 9.0 \times 10^{-4} M_\odot \text{yr}^{-1} \text{kpc}^{-2}$) for the normalization of the star formation law leads to differences of a few tenths of a dex between literature values and our total cold gas and molecular gas results. For example, $A_{\text{SF}} = 4.6 \times 10^{-3} M_\odot \text{yr}^{-1} \text{kpc}^{-2}$ (Bigiel et al. 2011) results in total gas surface densities differing by ~ 0.2 dex from results obtained using the parameter values presented in Table 1. This is a systematic shift upwards in indirect surface density over the entire range of surface densities probed. Changes in integrated indirect mass measures are of the order ~ 0.15 dex with respect to results obtained using the tabulated parameter values.

Offsets between molecular gas direct and indirect measures are more prominent, up to 0.5 dex for the integrated molecular gas masses when we adopt $A_{\text{SF}} = 4.6 \times 10^{-3} M_\odot \text{yr}^{-1} \text{kpc}^{-2}$. Adopting A_{SF} with values larger than presented in Table 1 results in a similar systematic shift downwards for predicted surface densities and integrated masses.

We applied an adapted formalism of the star formation law presented in Bigiel et al. (2008) to allow for higher SFE in dense regions (motivated by Daddi et al. 2010; Genzel et al. 2010). Adopting instead the standard SFE has no significant influence on the integrated cold gas and molecular gas predictions of local galaxies. Less concordance is reached between literature values and our predictions for the high redshift objects. We find a shift of approximately ~ 0.2 dex upwards away from the one-to-one line with respect to results obtained with the inclusion of an increased SFE at highest gas surface densities.

One of the key assumptions in this method is an exponential distribution of matter in the galaxy discs. SF occurs in molecular clouds (local clumps in the disc not following an exponential distribution), which could lead to a local underestimation of the cold gas surface density. Nevertheless, an exponential disc seems a valid approximation for star-forming galaxies on the main sequence (Wuyts et al. 2011), and the local clumps should average out when integrating over the disc. As we will discuss in Section 4.1, part of our COSMOS galaxy sample consists of quenched galaxies which fall off the main sequence. We are aware that these galaxies are not described by disks but that their light profiles are better described by a Vaucouleurs profile (Wuyts et al. 2011).

We assume that the gas in galactic discs is radially more extended than the stars. Varying the scale length of gas relative to stars, $\chi_{\text{gas}} \geq 1$, results in only subtle changes in the integrated total cold and molecular gas masses. However, decreasing the gas scale length to $\chi_{\text{gas}} < 1$ lowers the inferred integrated cold (molecular) gas masses. This difference can increase to ~ 0.25 (0.1) dex when $\chi_{\text{gas}} = 0.5$ with respect to results obtained using the parameters presented in Table 1.

Both the SFR and stellar mass are a function of the IMF. Changes in inferred total cold gas surface densities are less than 0.1 dex at the lowest gas surface densities when adopting a Salpeter IMF (Salpeter 1955) rather than the Chabrier IMF used above, and these changes become negligible at the highest surface densities. The integrated cold

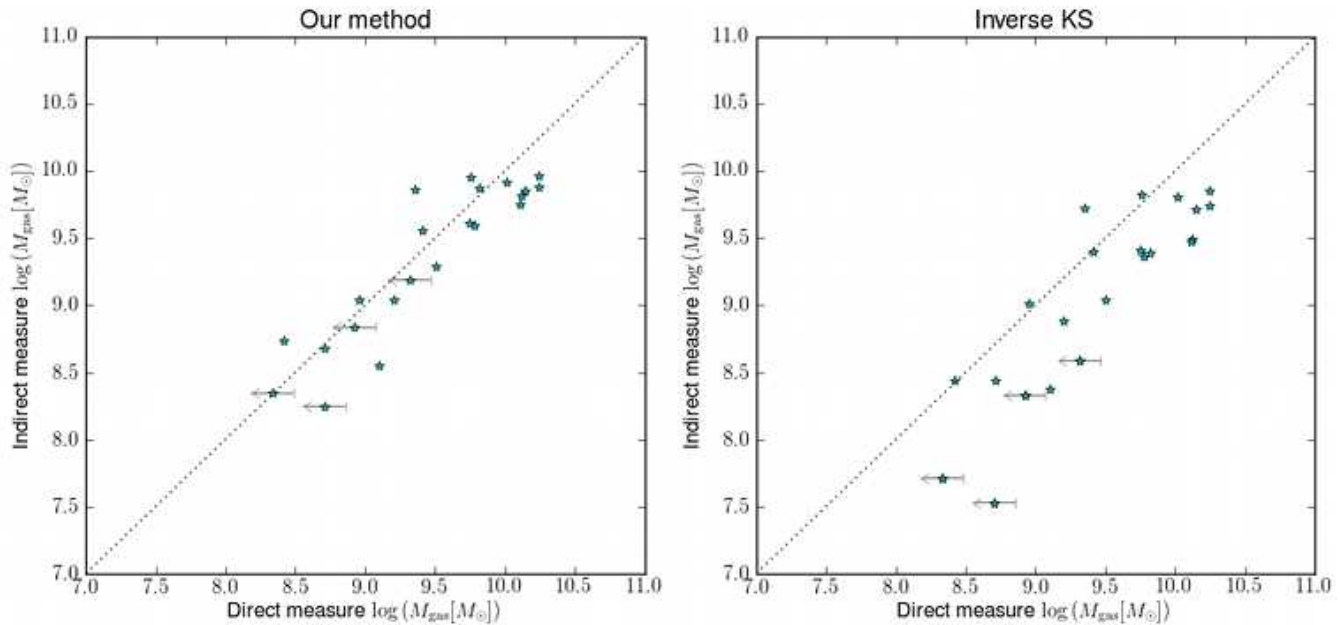


Figure 4. Indirect vs. direct measures of galaxy cold gas masses using our (left panel) and the KS (right panel) indirect gas method. No neutral gas measurements are available for the high-redshift galaxies, therefore only low-redshift galaxies are plotted. Our method finds good agreement with literature values, whereas the inverse KS method finds a deficit of total cold gas mass.

gas mass of the galaxies, as well as molecular gas surface densities and integrated masses do not change significantly when adopting a Salpeter IMF.

4 GAS EVOLUTION IN THE COSMOS SAMPLE

4.1 Sample

In order to determine the cold gas content and atomic and molecular composition of high-redshift galaxies, we used a galaxy sample taken from the Cosmic Evolution Survey (*COSMOS*; Scoville et al. 2007). The survey was designed to probe the evolution of galaxies, star formation, active galactic nuclei, and dark matter over the redshift range $z > 0.5 - 6$. These data comprise imaging and spectroscopy from X-ray to radio wavelengths including HST imaging and cover a two-square degree area on the sky.

We considered a catalogue of ~ 57000 galaxies with HST *I*-band magnitude $I_{AB} < 24$ mag in the redshift range $0.5 < z_{\text{phot}} < 2.0$ from the *COSMOS* survey. Photometric redshifts were obtained from Ilbert et al. (2009). SFRs are based on rest-frame UV fluxes, corrected using reddening values $E(B-V)$ obtained from Ilbert et al. (2009) for each individual galaxy. UV fluxes were converted into SFR following Kennicutt (1998a) for a Chabrier-IMF. We computed stellar masses using a multi-wavelength SED χ^2 fitting to the *COSMOS* photometry (*U* to *K*-band), applying the Bruzual (2007) templates fixed at the photometric redshifts of the sample objects. We used galaxy half light radii (r_{50}) taken from Scarlata et al. (2007) and Tasca et al. (2009).

The selection of galaxies in the *I*-band does not necessarily guarantee that all selected galaxies lie on the M_* –SFR plane. Our selection rather consists of both active star forming galaxies and galaxies already quenched. Inspection

of the data points out that quenched galaxies indeed are especially dominant towards the massive end of our galaxy sample ($\log M_* > 11 [M_\odot]$).

We warn the reader that the sampling of galaxies at $z > 1.5$ (and especially $z > 1.75$) is sparse, particularly at the low-mass end and one should use caution interpreting results in this redshift range.

4.2 Cold gas content

We present the derived total cold gas and molecular gas masses in Figures 5 and 6. Grey scales represent the log of the number of galaxies in each bin in the $M_{\text{gas}}(M_{H_2})$ – M_* plane, with 50, 16 and 84 percentiles over-plotted on the figure. Results are presented as a function of stellar mass in different redshift bins. Cold gas masses range from $\log M_{\text{gas}} \sim 10$ – $10.5 M_\odot$ at $z = 0.5$ – 0.75 with a peak around $\log M_* \sim 9.5 M_\odot$ to $\log M_{\text{gas}} \sim 11$ – $12 M_\odot$ at the highest redshifts in our sample peaking at a stellar mass of $\log M_* \sim 10.3 M_\odot$.

We find a large spread in molecular gas masses in the range of $\log M_{H_2} \sim 8.0$ – $11.0 M_\odot$ at the lowest redshifts in our sample and $\log M_{H_2} \sim 10.0$ – $11.5 M_\odot$ for the highest-redshift objects in our sample. The molecular gas masses peak at the same stellar masses as the integrated total cold gas masses.

Not only do the cold and molecular gas masses of galaxies at fixed stellar mass decrease with time, the largest gas reservoirs are always found in less- (stellar) massive objects. This trend suggests that (stellar) massive galaxies consumed their cold gas first, and only at later stages do less-massive galaxies fully consume their gas reservoir. We have explored the SFRs of galaxies of our sample galaxies as a function of redshift and found that for a given stellar mass, higher-

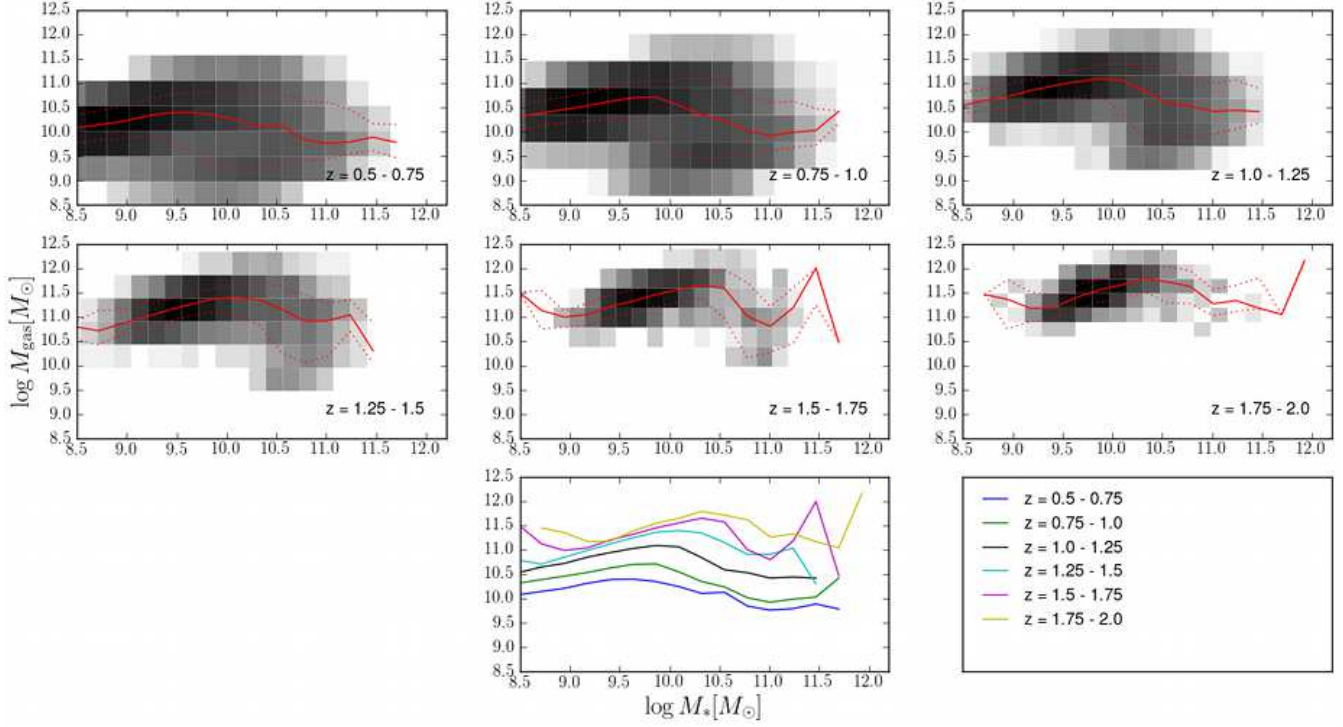


Figure 5. Total-cold mass gas as a function of stellar mass for different redshift bins. The grey shaded area shows the log of the number of galaxies in each gas/stellar mass bin, with the 50, 16 and 84 percentile curves shown with the red solid and dashed lines. The central bottom panel shows the 50 percentile curve for the data in each redshift bin. Bumps at the high-mass end in the highest redshift bins are due to ULIRGS (see Sec. 4.2)

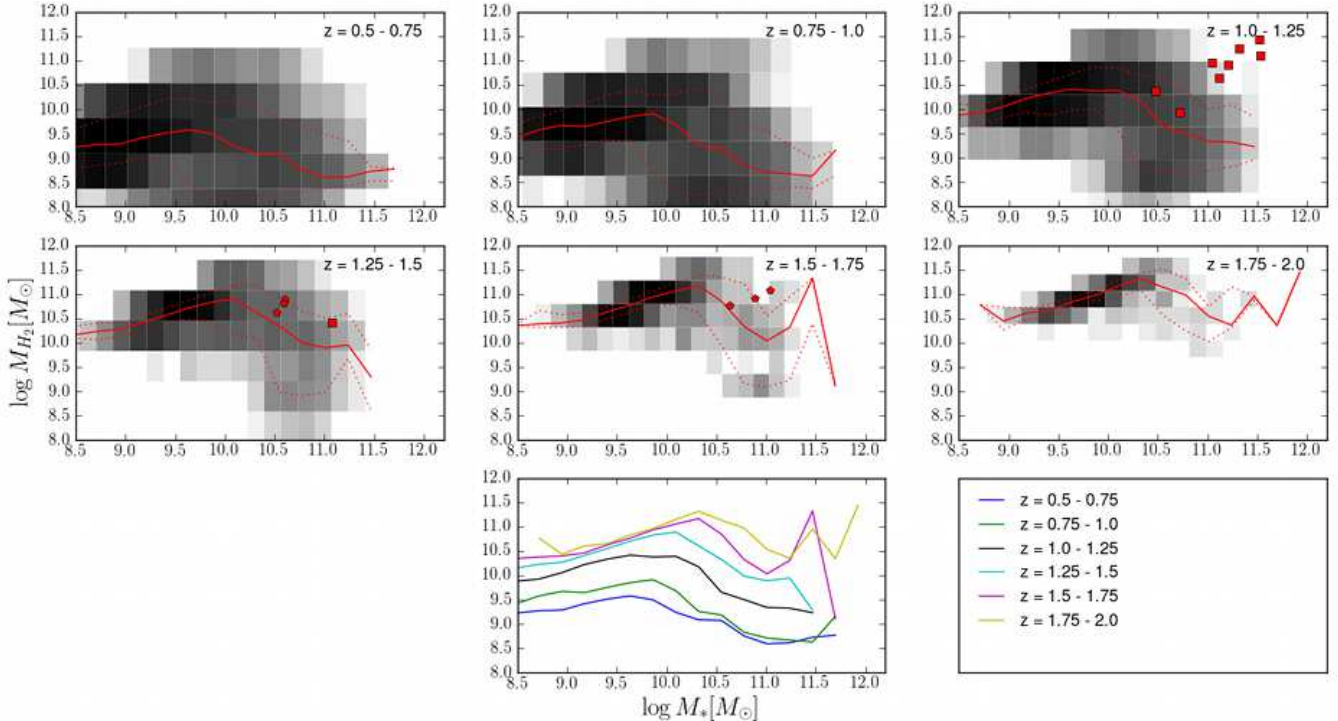


Figure 6. H_2 mass as a function of stellar mass for different redshift bins. The grey shaded area shows the log of the number of galaxies in each bin, with the 50, 16 and 84 percentile curves shown with the red solid and dashed lines. The central bottom panel shows the 50 percentile curve for the data in each redshift bin. Red squares and pentagons are literature values taken from Tacconi et al. (2010) and Daddi et al. (2010), respectively.

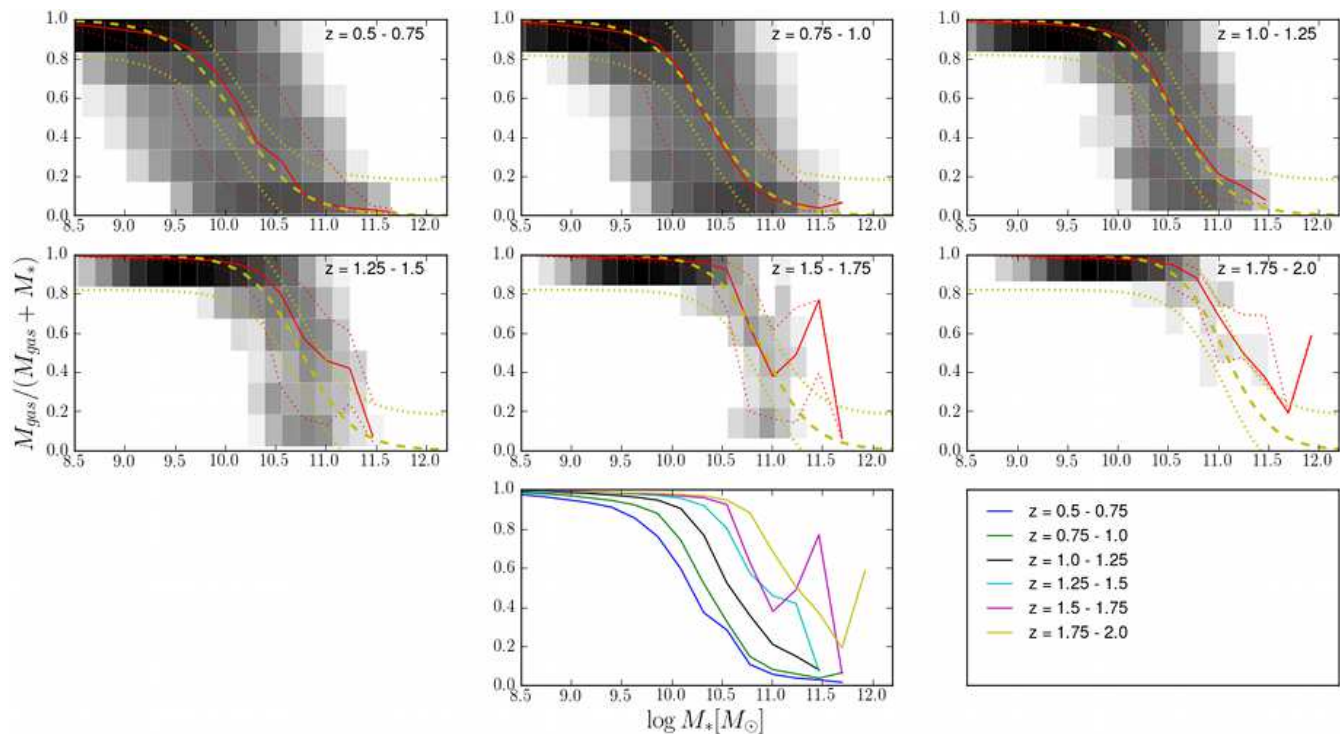


Figure 7. Total cold gas fraction (atomic plus molecular) as a function of stellar mass for different redshift bins. The grey shaded area shows the log of the number of galaxies in each bin, with the 50, 16 and 84 percentile curves shown with the red solid and dashed lines. The central bottom panel shows the 50 percentile curve for the data in each redshift bin. The dashed and dotted yellow lines represents the fit and one sigma scatter of Equation 10, respectively.

redshift objects have higher SFR (i.e., consume their gas faster) than their low-redshift counterparts.

We have superimposed observational results obtained by Daddi et al. (2010) and Tacconi et al. (2010) on Figure 6. We obtain good agreement between molecular gas masses computed with our method and observations extracted from the literature. Only in the redshift regime $z = 1.0$ – 1.25 do we compute a deficit of H_2 compared with results of Tacconi et al. (2010).

As pointed out in section 4.1, quenched galaxies make up for the dominant part of the massive objects in our sample and do not track the M_* –SFR plane. The Tacconi et al. (2010) galaxies on the other hand are actively forming stars and lie on the M_* –SFR plane. We find that these literature galaxies have specific SFR (SSFR) much higher than galaxies in the same redshift bin and with similar stellar masses in our *COSMOS* sample (> 1.0 dex). This difference in galaxy population (and consequently SSFR) can explain for the surplus of H_2 in literature galaxies compared to our predictions.

We find a few massive objects ($\log M_* \sim 11.5$ – $12.0 M_\odot$) with large total cold and molecular gas reservoirs ($\log M_{\text{gas}} \sim 12 M_\odot$), in disagreement with the declining trend in cold gas mass in less (stellar) massive objects. These are a handful of objects with SFRs of up to $\sim 200 M_\odot \text{yr}^{-1}$ and drive the increment of the 50 percentiles in the highest redshift bins. The objects are ultra luminous infrared galaxies (ULIRGS) with bright $24 \mu\text{m}$ intensities ($\sim 0.5 \text{ mJy}$), and are likely to have an AGN component. There are more ULIRGS in our sample, but it is the combination of high stellar mass and SFR which makes these galaxies show up so

prominently. If these galaxies indeed have an obscured AGN component, both the stellar mass and SFR could be overestimated which would be reflected in the cold and molecular gas content of these objects (Caputi et al. 2006).

4.3 Gas fraction

We present the gas fraction (fraction of all the baryonic mass which is in cold gas) of our galaxy sample as a function of stellar mass for different redshift bins in Figure 7. We find a clear trend in gas fraction and stellar mass for all redshift bins, with the highest gas fractions at low stellar masses. The gas fraction drops towards higher stellar masses and remains fairly constant around 0.0–0.1. More prominent, however, is the evolution of this trend with redshift (see the central panel in the third row of Figure 7). The stellar mass at which the gas fraction drops increases with increasing redshift, or, in other words, the gas fraction of galaxies at a given stellar mass increases with increasing redshift.

Figure 8 shows the fraction of molecular hydrogen H_2 with respect to the total stellar and molecular gas mass ($M_{H_2}/(M_{H_2} + M_*)$) as a function of stellar mass. This allows for a direct comparison with high-redshift galaxies from the literature. We find a trend between $M_{H_2}/(M_{H_2} + M_*)$ and stellar mass similar to the results of Figure 7. It also shows that $M_{H_2}/(M_{H_2} + M_*)$ at a fixed stellar mass increases with redshift. There is a large spread in $M_{H_2}/(M_{H_2} + M_*)$ at fixed stellar mass, especially in the lower redshift bins. As in Figure 6, we find good agreement between observations in the redshift range $1.25 < z < 1.75$ and our results. We find a

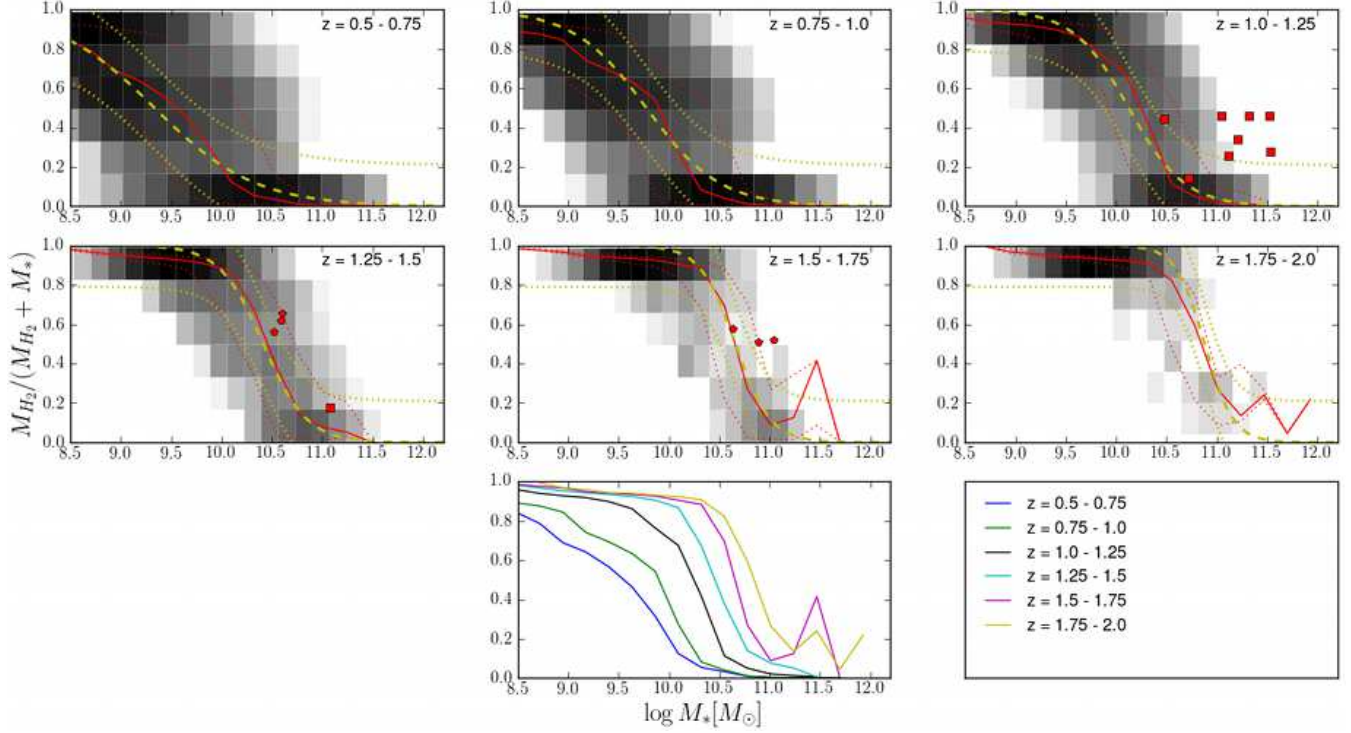


Figure 8. $M_{\text{H}_2}/(M_{\text{H}_2} + M_*)$ as a function of stellar mass for different redshift bins. The grey shaded area shows the log of the number of galaxies in each bin, with the 50, 16 and 84 percentile curves shown with the red solid and dashed lines. The central bottom panel shows the 50 percentile curve for the data in each redshift bin. Red squares and pentagons are literature values taken from Tacconi et al. (2010) and Daddi et al. (2010), respectively. The dashed and dotted yellow lines represents the fit and scatter (one sigma) of Equation 11, respectively.

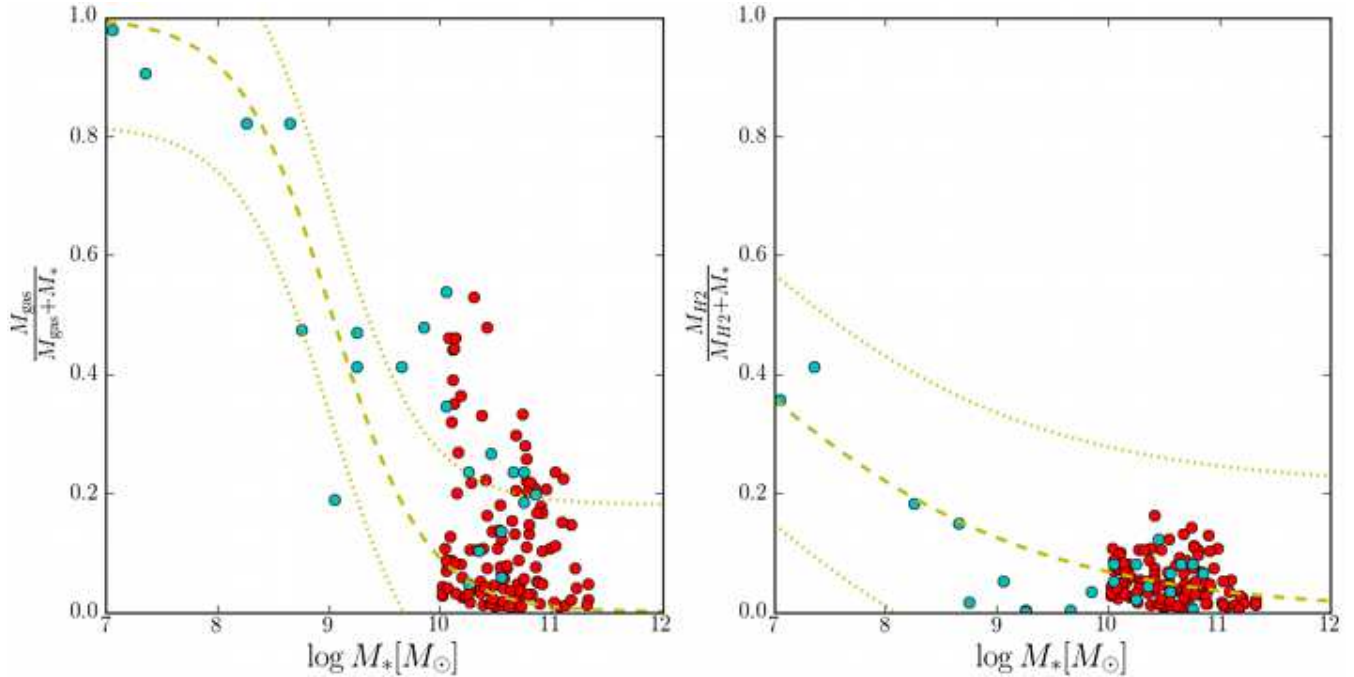


Figure 9. Total cold gas fraction (left hand panel) and $M_{\text{H}_2}/(M_{\text{H}_2} + M_*)$ (right hand panel) vs. stellar mass for local galaxies. Cyan and red dots are from Leroy et al. (2008) and Saintonge et al. (2011), respectively. The yellow dashed and dotted lines represent the fit and one sigma scatter of Equation 10 and 11, respectively. These were designed to match our galaxy sample and local data. Note that the actual scatter in $M_{\text{H}_2}/(M_{\text{H}_2} + M_*)$ for local galaxies is much less than the value obtained for Equation 11.

deficit in $M_{\text{H}_2}/(M_{\text{H}_2} + M_*)$ compared to observed objects at lower redshifts ($1 < z < 1.25$). As explained in the previous subsection this can be caused by differences in galaxy population. The peak in cold gas fraction and $M_{\text{H}_2}/(M_{\text{H}_2} + M_*)$ in the two highest redshift bins at high stellar masses represent the few galaxies with high SSFR which are classified as ULIRGS.

The cold gas fraction in our sampled redshift range can be characterized by a function of stellar mass and redshift, i.e.,

$$\frac{M_{\text{gas}}}{M_{\text{gas}} + M_*} = \frac{1}{\exp(\log M_* - A)/B + 1}, \quad (10)$$

where $A = 9.03(1 + \frac{z}{0.35})^{0.11}$ and $B = 0.42(1 + z)^{-0.56}$. This fitting formula was designed to match the 50 percentiles in 50 redshift bins between $0.5 < z < 1.7$ (where we sampled a large number of galaxies) and local data from Leroy et al. (2008) and Saintonge et al. (2011), respectively. We included local data with the aim of producing a representation of galaxy gas fraction valid for both local as distant galaxies. We find an approximately constant scatter of $\sigma = 0.18$. This slightly decreases towards the highest redshifts, but is likely an underestimation due to the low number of massive objects with large variations in their gas fractions. Although the function was not designed to match the highest redshift objects, it does a good job in reproducing their gas fraction. The left-hand panel of Fig. 9 shows the distribution of gas fraction with mass of local galaxies. We superimpose our fitting function and find that it describes the observed data fairly well.

Using the same approach we designed a fitting function to $M_{\text{H}_2}/(M_{\text{H}_2} + M_*)$, which is given by a similar equation

$$\frac{M_{\text{H}_2}}{M_{\text{H}_2} + M_*} = \frac{1}{\exp(\log M_* - A)/B + 1}, \quad (11)$$

where $A = 6.15(1 + \frac{z}{0.036})^{0.144}$ and $B = 1.47(1 + z)^{-2.23}$. This formula is a good quantitative representation of our full sample for local galaxies up to $z = 2$, and has a scatter of $\sigma = 0.21$ for our high-redshift galaxy sample (much less for the local objects).

Note that at stellar masses above $\log M_* > 11.0 [M_\odot]$ the presented fitting formulae do not apply for active star forming galaxies, but rather for an 'overall' galaxy population which consists of a mixture of star forming and quenched galaxies. We advise the reader to use the method presented in section 2 in the regime of massive, actively star forming galaxies.

4.4 H₂ fraction

Figure 10 shows the H₂ fraction of the cold gas (fraction of cold gas which is in a molecular state, $\text{H}_2/(\text{H}_2 + \text{HI})$) in our galaxy sample as a function of galaxy stellar mass, divided in different redshift bins. Galaxies have H₂ fractions spanning a range from nearly zero (hardly any H₂) to almost one (all the gas is in molecules) at all redshifts. There is nevertheless a (median) trend for the overall population of the galaxies.

We find the molecular fraction of the gas in most galaxies up to $z = 1$ to be around $f_{\text{H}_2} = 0.2$, with a minor decrease of the H₂ fraction with increasing stellar mass. The H₂ fraction increases up to values of $f_{\text{H}_2} = 0.3$ – 0.4 for most low-mass objects (below $\log M_*/M_\odot \sim 10$) at intermediate

redshifts ($z = 1$ – 1.5) and remains at this level at higher redshifts. The most-massive objects at the highest redshifts ($z = 1.5$ – 2.0) have molecular gas fractions of $f_{\text{H}_2} = 0.2$ – 0.3 and, similar to the galaxy gas fraction, show a small peak at $\log M_*/M_\odot \sim 11.5$ – 12.0 (caused by the ULIRGS). In general, massive galaxies reach low f_{H_2} values before less massive galaxies do. This trend is connected to the evolution of the gas fraction discussed in the previous subsection.

The described trend is reversed compared to the trend observed for local galaxies (i.e., f_{H_2} decreases with decreasing stellar mass, e.g., Leroy et al. 2008; Saintonge et al. 2011). This disagreement is driven by the quenched galaxies (with relatively low SFR and consequently relative low molecular content) which are dominant towards the massive end of our galaxy sample. We can decouple the mixture of passive and actively star-forming galaxies by considering galaxies at fixed SSFR. We should then expect to see the trend in f_{H_2} with stellar mass found in local galaxies, precisely as seen in Figure 11.

The molecular fraction of the cold gas with respect to the total cold gas in the galaxies for different redshift bins is presented in Figure 12. The figure shows a peak in H₂ fractions at higher redshift. At the lowest redshifts we see a gentle increase of H₂ fraction with increasing total cold gas mass, whereas at higher redshift the H₂ fraction peaks at a total cold gas mass of $\log M_{\text{gas}} \sim 10.7$ and decreases at higher masses.

This behavior demonstrates that the apportioning of the cold gas into atomic and molecular hydrogen is not driven by the cold gas budget available. This is not surprising as the Blitz & Rosolowsky (2006) formalism is based on the cold gas surface density.

4.5 Transition between gas and stellar dominated phase

The transition from a gas-dominated phase to a stellar-dominated phase can be used as a probe of the evolutionary stage of a galaxy. We plot the stellar masses of galaxies with gas fractions around ~ 0.5 (which marks the transition from gas to stellar dominated) as a function of redshift in Figure 13. We find that the typical stellar mass at this transition point decreases from $\log M_*(f_{\text{gas}}/M_\odot = 0.5) = 11.1$ at $z = 2.0$ to $\log M_*(f_{\text{gas}}/M_\odot = 0.5) = 10.1$ at $z = 0.5$. This decrease of an order of magnitude in stellar mass indicates that massive galaxies reach the transition from a gas- to a stellar-dominated phase well before less-massive galaxies.

5 DISCUSSION

We have shown that one can fairly accurately predict the total cold gas content of star forming galaxies as a function of their SFR, stellar mass and size. The cold gas can further be apportioned into atomic and molecular hydrogen. The key ingredient is a molecular gas-based star formation law combined with a prescription for the calculation of cold gas molecular fractions. In order to model a galaxy, the method assumes an exponential disc, integrated outwards to five times the stellar disc scale length. We obtain the best results when increasing the SFE in high cold gas surface density regions, especially important for high-redshift

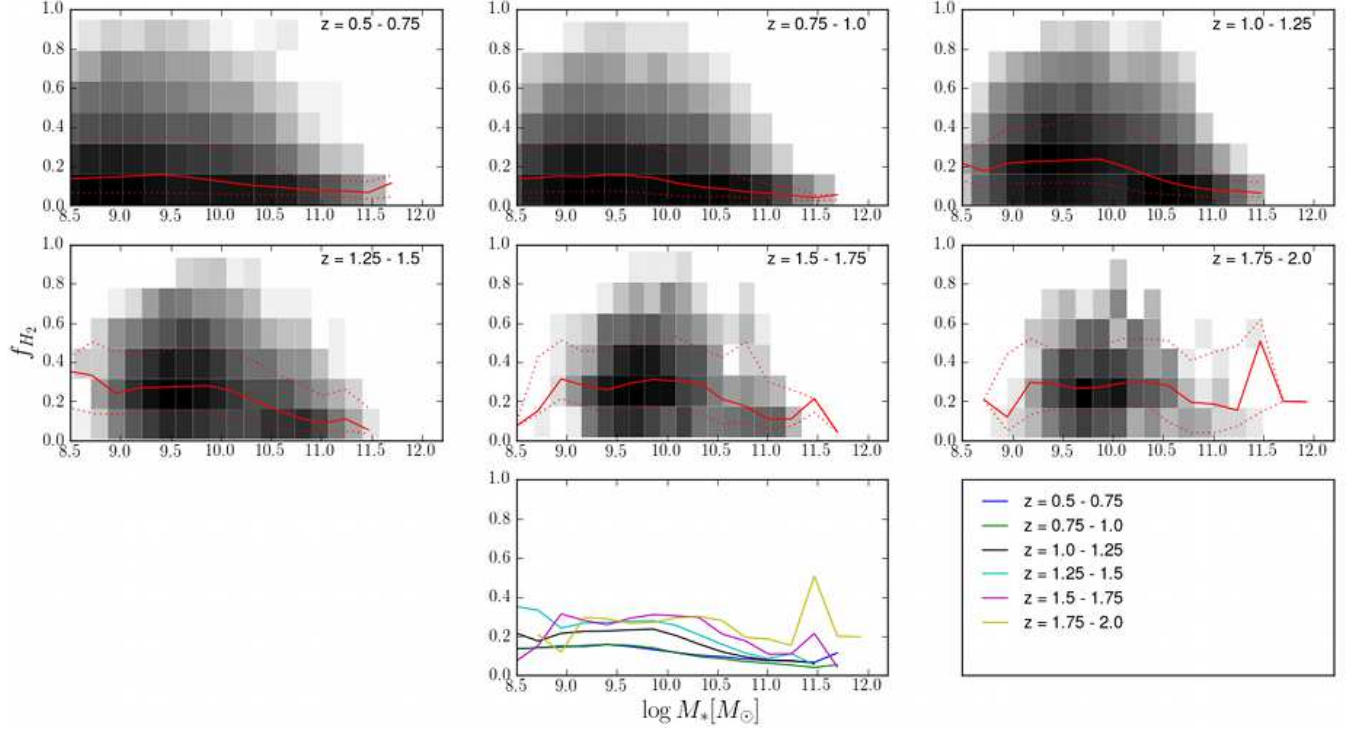


Figure 10. The fraction of H_2 in cold gas as a function of stellar mass for different redshift bins. The grey shaded area shows the log of the number of galaxies in each bin, with the 50, 16 and 84 percentile curves shown with the red solid and dashed lines. The central bottom panel shows the 50 percentile curve for the data in each redshift bin.

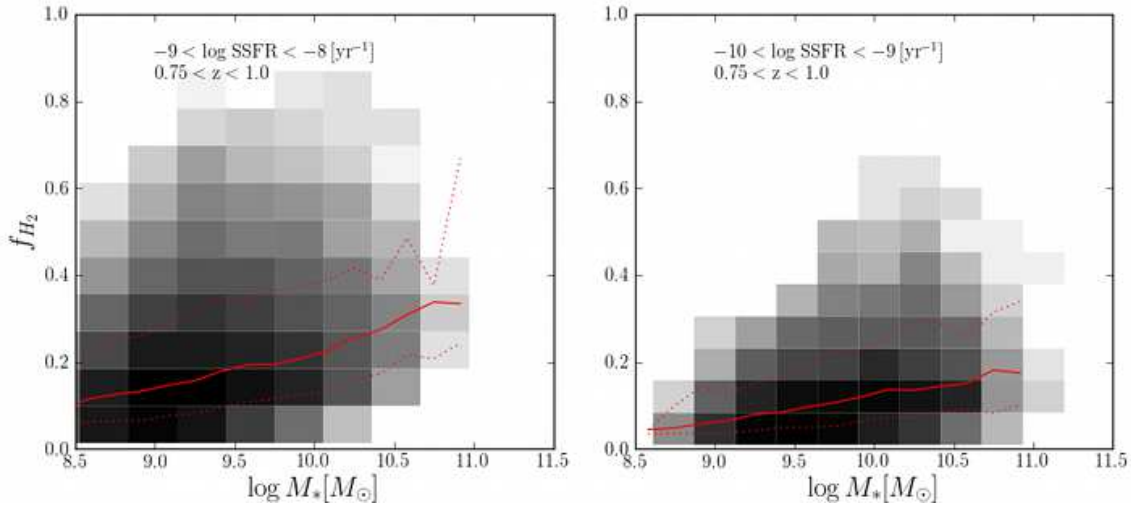


Figure 11. The fraction of H_2 in cold gas as a function of stellar mass for galaxies with a fixed SSFR. All galaxies have redshifts $0.75 < z < 1.0$. The grey shaded area shows the log of the number of galaxies in each bin, with the 50, 16 and 84 percentile curves shown with the red solid and dashed lines. Left panel: galaxies with $SSFR -9 < \log SSFR < -8 [yr^{-1}]$. Right panel: galaxies with $SSFR -10 < \log SSFR < -9 [yr^{-1}]$. Note that f_{H_2} decreases with decreasing stellar mass.

galaxies (see Sec. 3.3). This is in agreement with previous studies suggesting an increased SFE for dense high-redshift objects (Daddi et al. 2010; Genzel et al. 2010). It is outside the scope of this work to address the physical origin of this change in SFE.

Our method provides significantly better predictions of galaxy gas estimates than those derived from the KS law,

as can be seen from the comparison with direct galaxy gas measurements extracted from the literature. This is due to the break-down of the KS law at low surface densities, resulting in an underestimation of the cold gas necessary to sustain low SFR-rates. This break-down leads to significant changes when integrating over the outer parts of exponential discs.

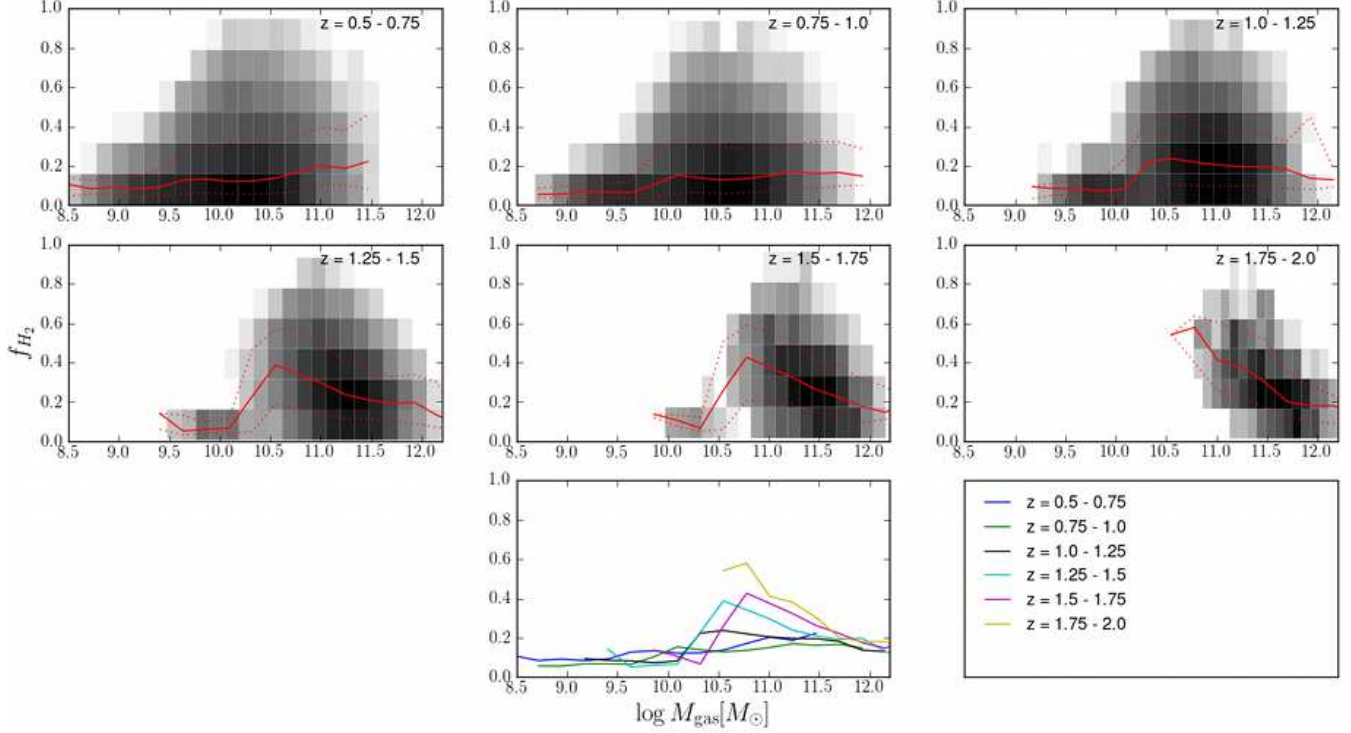


Figure 12. The fraction of H_2 in cold gas as a function of total gas mass for different redshift bins. The grey shaded area shows the log of the number of galaxies in each bin, with the 50, 16 and 84 percentile curves shown with the red solid and dashed lines. The central bottom panel shows the 50 percentile curve for the data in each redshift bin.

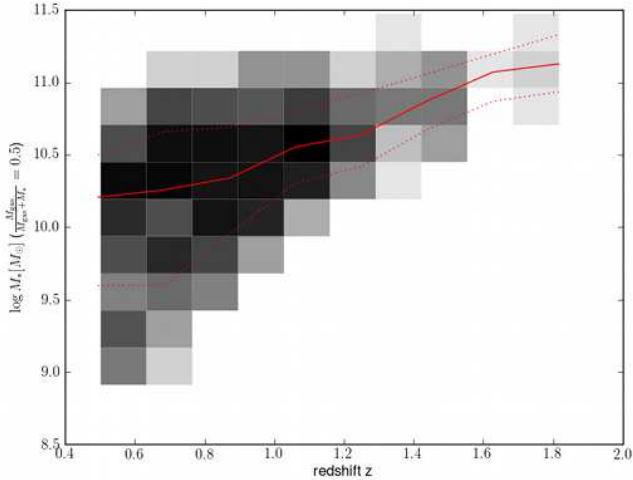


Figure 13. Stellar masses of galaxies with f_{gas} between 0.47 and 0.53 as a function of redshift. Grey scales show the log of the number of galaxies in each bin. Massive galaxies reach the transition point from a gas to a stellar dominated phase before less massive objects do.

Our method is applicable to low- and high-surface-density regions, as well as low- and high-redshift objects. Furthermore, the empirical success of the method gives support to our assumption of exponential profiles for the stellar and gaseous discs. Conversely, the method developed seems to be a good approach to compute SFRs from gas and stellar masses.

Despite the success of our method, it fails to properly

predict the molecular and total cold gas content of dwarf galaxies. As stated previously, Leroy et al. (2008) argue for an unaccounted-for reservoir of H_2 in these galaxies, possibly due to variations in the X_{CO} factor for dwarfs with respect to bigger spiral galaxies. It would therefore be worthwhile to address the X_{CO} conversion factor in dwarfs, in order to better understand the gas physics driving the partition of cold gas into atomic and molecular hydrogen. This will be crucial for a proper understanding of star formation at different stellar masses.

It is worthwhile to remember that we assume that the X_{CO} factor and IMF are universal. An evolving or variable IMF and/or X_{CO} could potentially lead to significant biases in our estimates. A much lower X_{CO} (suggested for starburst galaxies in e.g., Genzel et al. 2010) would result in much smaller H_2 reservoirs than predicted by our method. The IMF enters in converting the observed luminosities to stellar masses, as well as converting the observational tracers (such as H- α , UV or IR luminosity) to star formation rate. A top-heavy IMF would result in higher UV, IR or H- α luminosities for a given SFR, or correspondingly lower SFR estimates for a fixed observed luminosity. This would result in lower derived gas fractions.

Although the gas masses and molecular fractions presented here are obtained indirectly, our method allows for the first time the quantification of the cold gas and molecular gas for a large sample of galaxies at high redshift. This allows us to study the evolution of gas content in galaxies and track the relation between stellar and gas mass. High-redshift star-forming objects appear to be more gas-rich than lower redshift objects with similar stellar masses

(Fig. 5). We found that objects at $z \sim 2$ have a cold gas reservoir approximately thirty times larger than objects at $z \sim 0.5$ ($\log M_{\text{gas}}/M_{\odot} \sim 11.5$ versus $\log M_{\text{gas}}/M_{\odot} \sim 10.0$ at a stellar mass of $\log M_{*}/M_{\odot} = 8.5$) and that the largest gas reservoirs are found in progressively less-massive galaxies as a function of time. molecular gas reservoirs follow this behavior closely. These results indicate that massive galaxies consume or expel their gas earlier and at a higher rate than less-massive galaxies.

The galaxy gas fractions share the same evolution as total cold gas contents and decrease rapidly with decreasing redshift (Fig. 7). This trend is in good agreement with the few direct high redshift molecular gas measures available to date (Fig. 8). More striking is that massive galaxies reach low gas fractions (less than ~ 0.1) much sooner than less-massive objects.

We find a weak trend between stellar mass and the fraction of gas in molecular form (see Figure 10), such that massive galaxies have somewhat *lower* molecular fractions. In addition, there is a weak redshift trend in the sense that, at a fixed stellar mass, galaxies have higher molecular fractions at earlier times.

The apparent weak trend between stellar mass and the fraction of gas in molecular form is driven by the mixture of galaxies on the main-sequence and already quenched galaxies. We find that the molecular fraction of cold gas increases with stellar mass when we decouple this mixture (see Figure 11). This is in agreement with observations of local galaxies (Leroy et al. 2008; Saintonge et al. 2011).

We find no clear relationship between the molecular gas fraction and the total mass of cold gas available (see Figure 12). A large gas reservoir does not necessarily imply a high molecular fraction. However, we do find that the molecular fraction of a galaxy with fixed cold gas mass decreases with decreasing redshift. Under the assumption that cold gas is only eligible for star formation in a molecular state, these results indicate that high-redshift objects with a fixed cold gas content can transform more cold gas into stars than low redshift objects.

As discussed in Section 3.3 and 4.1, part of our galaxy sample falls off the main-sequence and is best described by a Vaucouleurs light profile rather than an exponential disc. These objects push to the limits of our method (which assumes an exponential disc) and one should interpret these with care.

In a hierarchical galaxy formation scenario, galaxy gas fractions represent the competition between gas inflow, outflow and consumption through SF (Davé, Finlator & Oppenheimer 2011). All the previously discussed processes hint at a similar general behavior of this competition with respect to host galaxy redshift and stellar mass. Massive galaxies consume or expel their gas before less-massive galaxies do. At a fixed stellar mass galaxies consume or expel more gas than they attract. This is all in agreement with Davé, Finlator & Oppenheimer (2011), who argue that the cosmic inflow rate of gas diminishes faster than the consumption rate. Furthermore, we find that the molecular fraction of the cold gas decreases with both stellar mass and time.

We present the transition from a gas to a stellar dominated galaxy in Figure 13. Galaxies that pass this transition point have expelled or consumed most of their gas and are

likely (unless they accrete a fresh supply of gas) to proceed towards a more quiescent phase of SF. We find that more massive galaxies reach a quiescent gas-poor state before less massive galaxies.

These processes are a reflection of downsizing in star formation, which can be defined as the declining mass of star-forming galaxies with decreasing redshift (Fontanot et al. 2009). Our results suggest that the slowly shrinking gas reservoirs, combined with lower molecular gas fractions, may drive the downsizing observed in star formation. It will be interesting to test this picture with future ‘direct’ observations of gas in galaxies at high redshift.

6 SUMMARY AND CONCLUSION

We developed a method to indirectly measure the total cold gas and molecular gas content of galaxies. We applied this method to a sample of galaxies from the *COSMOS* survey covering a redshift range of $0.5 \leq z \leq 2.0$. Since we obtained galaxy gas masses from their SFR, our results are effectively another way of representing SF and might seem redundant with other previous studies in the literature. It is therefore worthwhile to briefly summarize what we actually learned from this approach that we could not have concluded from the SFR alone. Our main results are:

- The gas content of a galaxy can be described using a combination of a molecular SF-law and a prescription to calculate the molecular fraction of cold gas, all under the assumption of a radial exponential profile for the gas and stars. Best results are obtained using a variable SFE. Conversely, this method can act as a scaling law relating the SFR surface density to the cold gas surface density of a galaxy. The method seems to be applicable to a large range of galaxy gas masses at both low and high redshift.
- The method presented allows us not only to predict the cold gas content but also to predict the molecular gas content of galaxies, and it is based on observed galaxy properties. These estimates can help us to interpret direct observations of molecular gas in galaxies at high redshift relative to the overall galaxy population.
- We find a strong trend between the gas content of a galaxy and its stellar mass with time. For a given stellar mass, the gas fraction of the galaxy decreases with decreasing redshift. On average, massive galaxies consume or expel their gas reservoir much earlier in the history of the Universe than less massive galaxies. This trend is not only observed in the cold gas content and gas fraction of the galaxies; it is also reflected in the molecular fraction of the cold gas, which gets smaller with time for a given stellar mass. This, in combination with low gas fractions, shows that the physics which suppress the formation of stars in massive galaxies with time is at least two-fold: galaxies run out of gas *and* molecules, but not necessarily at the same rate.
- The stellar mass at which galaxies become stellar-dominated decreases with time. This indicates that massive galaxies reach a gas-poor state before less massive objects.
- These results point towards a common trend: the more massive a galaxy, the sooner it consumes or expels its gas content. This trend is another manifestation of downsizing.

Although still indirect, these results point out that measuring the gas content of galaxies is of great use for developing a broader picture and better quantification of galaxy evolution. The method and results presented in this work are a first step in this direction and can help for the design of upcoming surveys. Furthermore, they provide useful constraints for cosmological galaxy formation models, particularly for the development of new models which include detailed tracking of multi-phase gas.

ACKNOWLEDGMENTS

We thank Françoise Combes and Andrew Baker for stimulating discussions, and Marco Spaans for a reading of the manuscript. GP acknowledges NOVA (Nederlandse Onderzoeksschool Voor Astronomie) for funding. KIC acknowledges the Leverhulme Trust for funding through the award of an Early Career Fellowship while this work was being done.

References

- Bigiel F., Leroy A., Walter F., Brinks E., de Blok W. J. G., Madore B., Thornley M. D., 2008, *AJ*, 136, 2846
- Bigiel F. et al., 2011, *ApJ*, 730, L13+
- Blitz L., Rosolowsky E., 2004, *ApJ*, 612, L29
- , 2006, *ApJ*, 650, 933
- Bolatto A. D., Leroy A. K., Rosolowsky E., Walter F., Blitz L., 2008, *ApJ*, 686, 948
- Bottema R., 1993, *A&A*, 275, 16
- Broeils A. H., Rhee M.-H., 1997, *A&A*, 324, 877
- Bruzual G., 2007, in *Astronomical Society of the Pacific Conference Series*, Vol. 374, *From Stars to Galaxies: Building the Pieces to Build Up the Universe*, A. Valenari, R. Tantalo, L. Portinari, & A. Moretti, ed., pp. 303–+
- Caputi K. I. et al., 2006, *ApJ*, 637, 727
- Chabrier G., 2003, *PASP*, 115, 763
- Cimatti A., Daddi E., Renzini A., 2006, *A&A*, 453, L29
- Cowie L. L., Songaila A., Hu E. M., Cohen J. G., 1996, *AJ*, 112, 839
- Daddi E. et al., 2010, *ApJ*, 713, 686
- Davé R., Finlator K., Oppenheimer B. D., 2011, *MNRAS*, 416, 1354
- Drory N., Bender R., Feulner G., Hopp U., Maraston C., Snigula J., Hill G. J., 2004, *ApJ*, 608, 742
- Drory N., Salvato M., Gabasch A., Bender R., Hopp U., Feulner G., Pannella M., 2005, *ApJ*, 619, L131
- Elmegreen B. G., 1989, *ApJ*, 338, 178
- , 1993, *ApJ*, 411, 170
- Erb D. K., Steidel C. C., Shapley A. E., Pettini M., Reddy N. A., Adelberger K. L., 2006, *ApJ*, 646, 107
- Faber S. M., Worthey G., Gonzales J. J., 1992, in *IAU Symposium*, Vol. 149, *The Stellar Populations of Galaxies*, B. Barbuy & A. Renzini, ed., pp. 255–+
- Fontanot F., De Lucia G., Monaco P., Somerville R. S., Santini P., 2009, *MNRAS*, 397, 1776
- Fu J., Guo Q., Kauffmann G., Krumholz M. R., 2010, *MNRAS*, 409, 515
- Genzel R. et al., 2010, *MNRAS*, 407, 2091
- Gnedin N. Y., Kravtsov A. V., 2011, *ApJ*, 728, 88
- Hopkins A. M., 2004, *ApJ*, 615, 209
- Hopkins A. M., Beacom J. F., 2006, *ApJ*, 651, 142
- Ilbert O. et al., 2009, *ApJ*, 690, 1236
- Kennicutt, Jr. R. C., 1998a, *ARA&A*, 36, 189
- , 1998b, *ApJ*, 498, 541
- Krumholz M. R., Dekel A., 2011, *ArXiv e-prints*
- Kuhlen M., Krumholz M., Madau P., Smith B., Wise J., 2011, *ArXiv e-prints*
- Lagos C. D. P., Baugh C. M., Lacey C. G., Benson A. J., Kim H.-S., Power C., 2011a, *MNRAS*, 1776
- Lagos C. D. P., Lacey C. G., Baugh C. M., Bower R. G., Benson A. J., 2011b, *MNRAS*, 416, 1566
- Leroy A. K., Walter F., Brinks E., Bigiel F., de Blok W. J. G., Madore B., Thornley M. D., 2008, *AJ*, 136, 2782
- Madau P., Ferguson H. C., Dickinson M. E., Giavalisco M., Steidel C. C., Fruchter A., 1996, *MNRAS*, 283, 1388
- Mannucci F. et al., 2009, *MNRAS*, 398, 1915
- McKee C. F., Ostriker E. C., 2007, *ARA&A*, 45, 565
- Obreschkow D., Rawlings S., 2009, *MNRAS*, 394, 1857
- Saintonge A. et al., 2011, *MNRAS*, 415, 32
- Salpeter E. E., 1955, *ApJ*, 121, 161
- Scarlata C. et al., 2007, *ApJS*, 172, 406
- Schmidt M., 1959, *ApJ*, 129, 243
- Schruba A. et al., 2011, *AJ*, 142, 37
- Scoville N. et al., 2007, *ApJS*, 172, 1
- Shostak G. S., van der Kruit P. C., 1984, *A&A*, 132, 20
- Solomon P. M., Rivolo A. R., Barrett J., Yahil A., 1987, *ApJ*, 319, 730
- Spaans M., Norman C. A., 1997, *ApJ*, 483, 87
- Tacconi L. J. et al., 2010, *Nature*, 463, 781
- Tasca L. A. M. et al., 2009, *A&A*, 503, 379
- Trager S. C., Faber S. M., Dressler A., 2008, *MNRAS*, 386, 715
- Trager S. C., Faber S. M., Worthey G., González J. J., 2000, *AJ*, 120, 165
- Wong T., Blitz L., 2002, *ApJ*, 569, 157
- Worthey G., Faber S. M., Gonzalez J. J., 1992, *ApJ*, 398, 69
- Wuyts S. et al., 2011, *ApJ*, 742, 96